

Reachability analysis of linear hybrid systems via block decomposition

Sergiy Bogomolov
Australian National University
Canberra, Australia

Marcelo Forets
Universidad de la República, CURE
Maldonado, Uruguay

Goran Frehse
ENSTA ParisTech - U2IS
Palaiseau Cedex, France

Kostiantyn Potomkin
Australian National University
Canberra, Australia

Christian Schilling
IST Austria
Klosterneuburg, Austria

ABSTRACT

Reachability analysis aims at identifying states reachable by a system within a given time horizon. This task is known to be computationally hard for hybrid systems. One of the main challenges is the handling of discrete transitions, including computation of intersections with invariants and guards. In this paper, we address this problem by proposing a state-space decomposition approach for linear hybrid systems. This approach allows us to perform most operations in low-dimensional state space, which can lead to significant performance improvements.

1 INTRODUCTION

A hybrid system [33] is a formalism for modeling cyber-physical systems. Reachability analysis is a rigorous way to reason about the behavior of hybrid systems.

In this paper, we describe a new reachability algorithm for linear hybrid systems, i.e., hybrid systems with dynamics given by linear differential equations and constraints given by linear inequalities. The key feature of our algorithm is that it performs computations in low-dimensional subspaces, which greatly improves scalability. To this end, we integrate a recent reachability algorithm for (purely continuous) LTI systems [11], which we call $Post_C^\square$ in the following, in a new algorithm for linear hybrid systems.

The $Post_C^\square$ algorithm decomposes the calculation of the reachable states into calculations in subspaces (called *blocks*). This decomposition has two benefits. The first benefit is that computations in lower dimensions are generally more efficient and thus the algorithm is highly scalable. The second benefit is that the analysis for different subspaces is decoupled; hence one can effectively skip the computations for dimensions that are of no interest (e.g., for a safety property).

Extending algorithms from purely continuous systems to hybrid systems is conceptually easy by adding a “hybrid loop” that interleaves a continuous-post algorithm and a discrete-post algorithm. If we consider $Post_C^\square$ as a black box, we can plug it into this hybrid loop, which we refer to as

$Post_H$ (cf. Section 3). However, there are two shortcomings. First, all operations aside from $Post_C^\square$ are still performed in high dimensions, and so $Post_H$ still suffers from scalability issues. Second, $Post_H$ does not make use of the decoupling of $Post_C^\square$ at all.

We demonstrate that, unlike in $Post_H$, it is possible to perform all computations in low dimensions (cf. Section 4). Surprisingly, we show that, in common cases, there is not even an additional approximation error. Furthermore, our algorithm makes proper use of the second benefit of $Post_C^\square$ by computing the reachable states only in specific dimensions whenever possible.

We implemented the algorithm in JuliaReach, a toolbox for reachability analysis [2, 12], and we evaluate the algorithm on several benchmark problems, including a 1024-dimensional hybrid system (cf. Section 5). Our algorithm outperforms the naive $Post_H$ and other state-of-the-art algorithms by several orders of magnitude.

To summarize, we show how to integrate the decomposed reachability algorithm for LTI systems from [11] into a decomposed reachability algorithm for linear hybrid systems. The key insights are (1) to exploit the decomposed structure of the reachable states to perform all operations in low dimensions and (2) to only compute the reachable states in specific dimensions whenever possible.

Related work

Decomposition. Hybrid systems given as a network of components can be explored efficiently in a symbolic way, e.g., using bounded model checking [14]. We consider a decomposition in the continuous state space. Schupp et al. perform such a decomposition by syntactic independence [43], which corresponds to dynamics matrices of block-diagonal form.

For purely continuous systems there exist various decomposition approaches. In this work we build on [11] for LTI systems, which decomposes the system into blocks and exploits the linear dynamics to avoid the wrapping effect. Other approaches for LTI systems are based on Krylov subspace

approximations [32], time-scale decomposition [19, 28], similarity transformations [35, 36], projectahedra [29, 45], and sub-polyhedra abstract domains [44]. Approaches for non-linear systems are based on projections with differential inclusions [8], Hamilton-Jacobi methods [16, 41], and hybridization with iterative refinement [17].

Lazy flowpipe computation. The support-function representation of convex sets can be used to represent a flowpipe (a sequence of sets that covers the behaviors of a system) symbolically [26]. Only sets that are of interest, e.g., those that intersect with a constraint, need then be approximated [23]. Using our decomposition approach, we can even avoid the symbolic computation in dimensions that are irrelevant to the intersection. Our approach is independent of the set representation, so it can also be applied in analyses based on, e.g., zonotopes [4, 6, 25, 27]. Given a linear switching system with a hyperplanar state-space partition, Hamadeh and Goncalves compute ellipsoidal over- and underapproximations of the reach set on the partition borders, without computing the full reach set [31].

Intersection of convex sets. Performing intersections in low dimensions allows for efficient computations that are not possible in high dimensions. For example, checking for emptiness of a polyhedron in constraint representation is a feasibility linear program, which can be solved in weakly polynomial time, but solutions in strongly polynomial time are only known in two dimensions [34].

In the context of hybrid-system reachability, computing intersections is considered a major challenge because it usually requires a conversion from efficient set representations (like zonotopes, support function, or Taylor models) to polytopes and back, which often involves an additional approximation. Below we summarize how other approaches tackle the intersection problem.

A coarse approximation of the intersection with a guard can be obtained by only detecting a nonempty intersection (which is generally easier to do) and then taking the original set as overapproximation [42]. In general, the intersection between a polytope and polyhedral constraints (invariants and guards) can be computed exactly, but such an approach is not scalable [18]. Girard and Le Guernic consider hyperplanar constraints where reachable states are either zonotopes, in which case they work in a two-dimensional projection [27], or general polytopes [30, 37]. The tool SpaceEx approximates the intersection of polytopes and general polyhedra using template directions [21]. Frehse and Ray propose an optimization scheme for the intersection of a compact set \mathcal{X} , represented by its support function, and a polyhedron \mathcal{Y} , and this scheme is exact if \mathcal{X} is a polytope [23]. The problem of performing intersections can also be cast in terms

of finding separating hyperplanes [13, 20]. Althoff et al. approximate zonotopes by parallelotopes before considering the intersection [6]. For must semantics, Althoff and Krogh use constant-dynamics approximation and obtain a nonlinear mapping [5]. Under certain conditions, Bak et al. apply a model transformation by replacing guard constraints by time-triggered constraints, for which intersection is easy [9].

2 PRELIMINARIES

We introduce some notation. The real numbers are denoted by \mathbb{R} . Given two vectors $x, y \in \mathbb{R}^n$, their dot product is $\langle x, y \rangle := \sum_{i=1}^n x_i \cdot y_i$. For $p \geq 1$, the p -norm of a matrix $A \in \mathbb{R}^{n \times n}$ is denoted $\|A\|_p$. The diameter of a set $\mathcal{X} \subseteq \mathbb{R}^n$ is $\Delta_p(\mathcal{X}) := \sup_{x, y \in \mathcal{X}} \|x - y\|_p$. The n -dimensional unit ball of the p -norm is $\mathcal{B}_p^n := \{x \in \mathbb{R}^n \mid 1 \geq \|x\|_p\}$. An n -dimensional half-space is the set $\{(a, x) \leq b \mid x \in \mathbb{R}^n\}$ parameterized by $a \in \mathbb{R}^n, b \in \mathbb{R}$. A polyhedron is an intersection of finitely many half-spaces, and a polytope is a bounded polyhedron.

Given two sets $\mathcal{X} \subseteq \mathbb{R}^n$ and $\mathcal{Y} \subseteq \mathbb{R}^m$, a scalar $\lambda \in \mathbb{R}$, a matrix $A \in \mathbb{R}^{n \times n}$, and a vector $b \in \mathbb{R}^n$, we use the following operations on sets: scaling $\lambda\mathcal{X} := \{\lambda x \mid x \in \mathcal{X}\}$, linear map $A\mathcal{X} := \{Ax \mid x \in \mathcal{X}\}$, Minkowski sum $\mathcal{X} \oplus \mathcal{Y} := \{x + y \mid x \in \mathcal{X} \text{ and } y \in \mathcal{Y}\}$ (if $n = m$), affine map $(A, b) \odot \mathcal{X} := A\mathcal{X} \oplus \{b\}$, Cartesian product $\mathcal{X} \times \mathcal{Y} := \{(x, y) \mid x \in \mathcal{X}, y \in \mathcal{Y}\}$, intersection $\mathcal{X} \cap \mathcal{Y} := \{z \mid z \in \mathcal{X}, z \in \mathcal{Y}\}$ (if $n = m$), and convex hull $\text{CH}(\mathcal{X}) := \{\lambda \cdot x + (1 - \lambda) \cdot y \mid x, y \in \mathcal{X}, 0 \leq \lambda \leq 1\}$.

Given two sets $\mathcal{X}, \mathcal{Y} \subseteq \mathbb{R}^n$, the Hausdorff distance is defined as

$$d_H^p(\mathcal{X}, \mathcal{Y}) := \inf_{\varepsilon \in \mathbb{R}} \left\{ \mathcal{Y} \subseteq \mathcal{X} \oplus \varepsilon \mathcal{B}_p^n \text{ and } \mathcal{X} \subseteq \mathcal{Y} \oplus \varepsilon \mathcal{B}_p^n \right\}.$$

Let $C_n \subseteq 2^{\mathbb{R}^n}$ be the set of n -dimensional compact and convex sets. For a nonempty set $\mathcal{X} \in C_n$, the support function $\rho_{\mathcal{X}} : \mathbb{R}^n \rightarrow \mathbb{R}$ is defined as

$$\rho_{\mathcal{X}}(d) := \max_{x \in \mathcal{X}} \langle d, x \rangle.$$

The Hausdorff distance of two sets $\mathcal{X}, \mathcal{Y} \in C_n$ with $\mathcal{X} \subseteq \mathcal{Y}$ can alternatively be expressed in terms of the support function as

$$d_H^p(\mathcal{X}, \mathcal{Y}) = \max_{\|d\|_p \leq 1} \rho_{\mathcal{Y}}(d) - \rho_{\mathcal{X}}(d).$$

We use β to denote the number of blocks in a partition. Let $\{\pi_j\}_{j=1}^\beta$ be a set of (contiguous) projection matrices that partition a vector $x \in \mathbb{R}^n$ into $x = [\pi_1 x, \dots, \pi_\beta x]$. Given a set \mathcal{X} and projection matrices $\{\pi_j\}_{j=1}^\beta$, we call $\pi_1 \mathcal{X} \times \dots \times \pi_\beta \mathcal{X}$ the Cartesian decomposition with the block structure induced by the π_j . We refer to $\pi_j \mathcal{X}$ as a *block* of \mathcal{X} and typically write $\widehat{\mathcal{X}}$ to indicate a decomposed set (i.e., a Cartesian product of lower-dimensional sets). For instance, given a nonempty set

$\mathcal{X} \in C_n$, its box approximation is the Cartesian decomposition into intervals (i.e., one-dimensional blocks). We can bound the approximation error by the radius of \mathcal{X} .

PROPOSITION 2.1. *Let $\mathcal{X} \in C_n$ be nonempty, $p = \infty$, $r_{\mathcal{X}}^p$ be the radius of the box approximation of \mathcal{X} , and let π_j be appropriate projection matrices. Then $d_H^p(\mathcal{X}, \times_j \pi_j \mathcal{X}) \leq \|r_{\mathcal{X}}^p\|_p$.*

2.1 LTI systems

An n -dimensional LTI system (A, B, \mathcal{U}) , with matrices $A \in \mathbb{R}^{n \times n}$, $B \in \mathbb{R}^{n \times m}$, and input domain $\mathcal{U} \in C_m$, is a system of ODEs of the form

$$\dot{x}(t) = Ax(t) + Bu(t), \quad u(t) \in \mathcal{U}. \quad (1)$$

We denote the set of all n -dimensional LTI systems by \mathcal{L}_n . From now on, a vector $x \in \mathbb{R}^n$ is also called a (continuous) state. Given an initial state $x_0 \in \mathbb{R}^n$ and an input signal u such that $u(t) \in \mathcal{U}$ for all t , a *trajectory* of (1) is the unique solution $\xi_{x_0, u} : \mathbb{R}_{\geq 0} \rightarrow \mathbb{R}^n$ with

$$\xi_{x_0, u}(t) = e^{At} x_0 + \int_0^t e^{A(t-s)} Bu(s) ds.$$

Given an LTI system (A, B, \mathcal{U}) and a set $\mathcal{X}_0 \in C_n$ of initial states, the *continuous-post operator*, $Post_C$, computes the set of reachable states for all input signals u over \mathcal{U} :

$$Post_C((A, B, \mathcal{U}), \mathcal{X}_0) := \{\xi_{x_0, u}(t) \mid t \geq 0, x_0 \in \mathcal{X}_0, u(s) \in \mathcal{U} \text{ for all } s\}.$$

2.2 Linear hybrid systems

We briefly introduce the syntax of linear hybrid systems used in this work and refer to the literature for the semantics [7, 33]. An n -dimensional linear hybrid system is a tuple $\mathcal{H} = (Var, Loc, Flow, Inv, Grd, Asgn)$ with variables $Var = \{x_1, \dots, x_n\}$, a finite set of locations Loc , two functions $Flow : Loc \rightarrow \mathcal{L}_n$ and $Inv : Loc \rightarrow C_n$ that respectively assign continuous dynamics and an invariant to each location, and two functions $Grd : Loc \times Loc \rightarrow C_n$ and $Asgn : Loc \times Loc \rightarrow \mathbb{R}^{n \times n} \times \mathbb{R}^n$ that respectively assign a guard and an assignment in the form of a deterministic affine map to each pair of locations. If $Grd((\ell, \ell')) \neq \emptyset$, we call (ℓ, ℓ') a (discrete) transition.

Let $\mathcal{H} = (Var, Loc, Flow, Inv, Grd, Asgn)$ be a linear hybrid system. A (symbolic) state of \mathcal{H} is a pair $(\ell, \mathcal{X}) \in Loc \times 2^{\mathbb{R}^n}$. The *discrete-post operator*, $Post_D$, maps a symbolic state to a set of symbolic states by means of discrete transitions:

$$Post_D((\ell, \mathcal{X})) := \bigcup_{\ell' \in Loc} \{(\ell', Asgn((\ell, \ell'))) \odot (\mathcal{X} \cap Inv(\ell) \cap Grd((\ell, \ell'))) \cap Inv(\ell')\} \quad (2)$$

The *reach set* of \mathcal{H} from a set of initial symbolic states \mathcal{R}_0 of \mathcal{H} is the smallest set \mathcal{R} of symbolic states such that

$$\mathcal{R}_0 \cup \bigcup_{(\ell, \mathcal{X}) \in \mathcal{R}} Post_D((\ell, Post_C(Flow(\ell), \mathcal{X}))) \subseteq \mathcal{R}. \quad (3)$$

Safety properties can be given as a set of symbolic error states that should be avoided and be encoded as the guard of a transition to a new error location. In our implementation we can also check inclusion in the safe states and we do not use the encoding with additional transitions.

3 REACHABILITY ANALYSIS OF LINEAR HYBRID SYSTEMS

Our reachability algorithm for linear hybrid systems integrates the algorithm from [11], which implements $Post_C$ for LTI systems in a compositional way. In this section, we first recall the algorithm from [11], which from now on we call $Post_C^\square$ for convenience. Two important properties of $Post_C^\square$ are that (1) the output is a sequence of *decomposed* sets and that (2) this sequence is computed in low dimensions.

After explaining the algorithm $Post_C^\square$, we incorporate it in a standard reachability algorithm for linear hybrid systems. However, this standard reachability algorithm will not make use of the above-mentioned properties. This will motivate our new algorithm (presented in Section 4), which is a modification of this standard reachability algorithm to make optimal use of these properties.

3.1 Decomposed reachability analysis of LTI systems

The decomposition-based approach [11] follows a flowpipe-construction scheme using time discretization, which we shortly recall here. Given an LTI system (A, B, \mathcal{U}) and a set of initial (continuous) states \mathcal{X}_0 , by fixing a time step δ we first compute a set $\mathcal{X}(0)$ that overapproximates the reach set up to time δ , a matrix $\Phi = e^{A\delta}$ that captures the dynamics of duration δ , and a set \mathcal{V} which overapproximates the effect of the inputs up to time δ . We obtain an overapproximation of the reach set in time interval $[k\delta, (k+1)\delta]$, for step $k > 0$, with

$$\mathcal{X}(k) := \Phi \mathcal{X}(k-1) \oplus \mathcal{V} = \Phi^k \mathcal{X}(0) \oplus \bigoplus_{j=0}^{k-1} \Phi^j \mathcal{V}.$$

Algorithm $Post_C^\square$ decomposes this scheme. Fixing some block structure, let $\widehat{\mathcal{X}}(0) := \mathcal{X}_1(0) \times \dots \times \mathcal{X}_\beta(0)$ be the corresponding Cartesian decomposition of $\mathcal{X}(0)$. We compute a sequence $\widehat{\mathcal{X}}(k) := \mathcal{X}_1(k) \times \dots \times \mathcal{X}_\beta(k)$ such that $\mathcal{X}(k) \subseteq \widehat{\mathcal{X}}(k)$ for every k . Each low-dimensional set $\mathcal{X}_i(k)$ is computed as

$$\mathcal{X}_i(k) := \bigoplus_{j=1}^{\beta} (\Phi^k)_{ij} \mathcal{X}_j(0) \oplus \bigoplus_{j=0}^{k-1} [(\Phi^j)_{i1} \dots (\Phi^j)_{i\beta}] \mathcal{V}.$$

The above sequences $\mathcal{X}(k)$ resp. $\widehat{\mathcal{X}}(k)$ are called flowpipes.

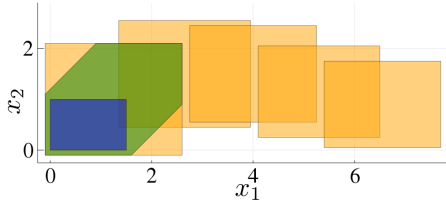


Figure 1. Starting from the set of initial states \mathcal{X}_0 (blue set), we first compute the set $\mathcal{X}(0)$ by time discretization (green set), then decompose the set into intervals and obtain $\widehat{\mathcal{X}}(0)$ (orange box around $\mathcal{X}(0)$), and finally compute the (decomposed) flowpipe $\widehat{\mathcal{X}}(1), \dots, \widehat{\mathcal{X}}(4)$ by propagating each of the intervals (other orange sets).

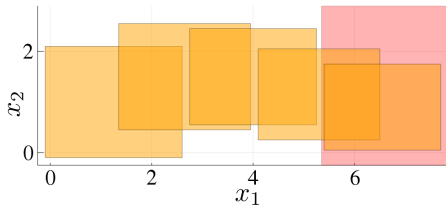


Figure 2. The flowpipe from Figure 1 together with a guard (red).

Example. We illustrate the algorithms with a running example throughout the paper. For illustration purposes, the example is two-dimensional (and hence we decompose into one-dimensional blocks, but we emphasize that the approach also generalizes to higher-dimensional decomposition) and we consider a hybrid system with only a single location and one transition (a self-loop). Figure 1 depicts the flowpipe construction for the example.

3.2 Reachability analysis of linear hybrid systems

We now discuss a standard reachability algorithm for hybrid systems. Essentially, this algorithm interleaves the operators $Post_C$ and $Post_D$ following (3) until it finds a fixpoint. Here we use $Post_C^\square$ as the continuous-post operator.

We first compute a flowpipe $\widehat{\mathcal{X}} = \widehat{\mathcal{X}}(0), \dots, \widehat{\mathcal{X}}(N)$ using $Post_C^\square$ as described above. Then we use $Post_D$ to take a discrete transition. According to (2), we want to compute $((A, b) \odot (\widehat{\mathcal{X}} \cap \mathcal{I}_1 \cap \mathcal{G})) \cap \mathcal{I}_2$, where (A, b) is a deterministic affine map. Frehse and Ray showed that for such maps the term can be simplified to

$$(A, b) \odot (\widehat{\mathcal{X}} \cap \mathcal{G}^*) \quad (4)$$

where the set \mathcal{G}^* can be statically precomputed [23], which is usually easy because the sets \mathcal{I}_1 , \mathcal{G} , and \mathcal{I}_2 are given as polyhedra in constraint representation. Hence we ignore invariants in the rest of the presentation.

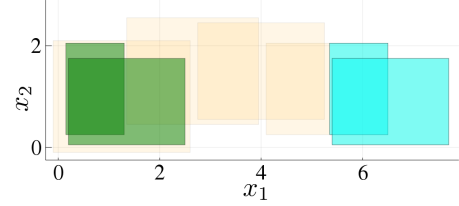


Figure 3. The assignment shifts the intersection of the flowpipe and the guard from Figure 2 (cyan) to the green sets, which are both contained in the first set of the original flowpipe.

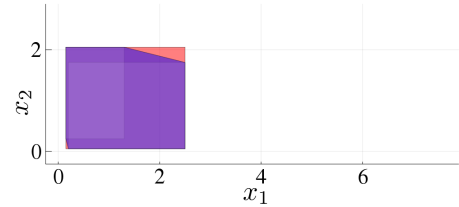


Figure 4. Approximation of the union of the green sets from Figure 3 using the convex hull (purple) and the decomposed convex hull (red).

Example. We continue in Figure 2 with the flowpipe from before. The guard \mathcal{G} is a half-space that is constrained in dimension x_1 and unconstrained in dimension x_2 . Only the last two sets in the flowpipe intersect with the guard. The assignment here is a translation in dimension x_1 . The resulting intersection, before and after the translation, is depicted in Figure 3.

Finally, the algorithm checks for a fixpoint, i.e., for inclusion of the symbolic states we computed with $Post_D$ in previously-seen symbolic states.

Example. The green set in Figure 3 shows that the two sets we obtained from $Post_D$ are contained in $\widehat{\mathcal{X}}(0)$ computed before. (Recall that in this example we only consider a single location; hence the inclusion holds for symbolic states.)

The steps outlined above describe one iteration of the standard reachability algorithm. Each symbolic state for which the fixpoint check was negative spawns a new flowpipe. Since this can lead to a combinatorial explosion, one typically applies a technique called *clustering* (cf. [21]), where symbolic states are merged after the application of $Post_D$. Here we consider clustering with a convex hull.

Example. Assume that the fixpoint check above was negative for both sets that we tested. In Figure 4 we show the convex hull of the sets in purple.

Up to now, we have seen a standard incorporation of an algorithm for the continuous-post operator $Post_C$ (for which

we used $Post_C^\square$ into a reachability algorithm for hybrid systems. Observe that $Post_C$ was used as a black box. Consequently, we could not make use of the properties of the specific algorithm $Post_C^\square$. In particular, apart from $Post_C^\square$, we performed all computations in high dimensions. In the next section, we describe a new algorithm that instead performs all computations in low dimensions.

4 DECOMPOSED REACHABILITY ANALYSIS

We now present a new, decomposed reachability algorithm for linear hybrid systems. The algorithm uses $Post_C^\square$ for computing flowpipes and has two major performance improvements over the previous algorithm.

Recall that $Post_C^\square$ computes flowpipes consisting of decomposed sets. The first improvement is to exploit the decomposed structure in order to perform all other operations (intersection, affine map, inclusion check, and convex hull) in low dimensions.

The second improvement is to compute flowpipes in a sparse way. Roughly speaking, we are only interested in those dimensions of a flowpipe that are relevant to determine intersection with a guard. Hence we only need to compute the other dimensions of the flowpipe after we detected such an intersection.

The algorithm starts as before: Given an initial (symbolic) state, we compute $\mathcal{X}(0)$ (discretization) and decompose the set to obtain $\widehat{\mathcal{X}}(0)$. Next we want to compute a flowpipe, and this is where we deviate from the previous algorithm.

4.1 Computing a sparse flowpipe

We hook into $Post_C^\square$ in order to control the dimensions of the flowpipe. Recall that the black-box version of $Post_C^\square$ computed the flowpipe $\widehat{\mathcal{X}}(k) = \mathcal{X}_1(k) \times \dots \times \mathcal{X}_\beta(k)$ for $k = 1, \dots, N$, i.e., in all dimensions. This is usually not necessary for detecting an intersection with a guard. We will discuss this formally below, but want to establish some intuition first. Recall the running example from before. The guard was only constrained in dimension x_1 . This means that the bounds of the sets $\widehat{\mathcal{X}}(k) = \mathcal{X}_1(k) \times \mathcal{X}_2(k)$ in dimension x_2 are irrelevant. Consequently, we do not need to compute the sets $\mathcal{X}_2(k)$ at all (at least for the moment). We only compute those dimensions of a flowpipe that are necessary to determine intersection with the guards. Identifying these dimensions and projecting the guards accordingly has to be performed only once per transition and is often just a syntactic procedure.

Example. As discussed, we only compute the flowpipe $\mathcal{X}_1(1), \dots, \mathcal{X}_1(4)$ for the first block (in dimension x_1), i.e., a

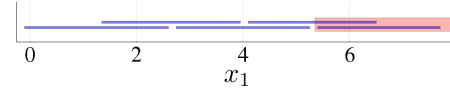


Figure 5. The flowpipe from Figure 1 in dimension x_1 only consists of intervals (blue). The constraint \mathcal{G}_1 (red) is the guard \mathcal{G} projected to x_1 . For better visibility, we draw the sets thicker and add a slight offset to some of the intervals.

sequence of intervals, which is depicted in Figure 5. Projecting the guard to x_1 , we obtain a ray \mathcal{G}_1 . As expected, we observe an intersection with the guard for the same time steps as before (namely steps $k = 3$ and $k = 4$).

4.2 Decomposing an intersection

Next we discuss how to compute an intersection $\widehat{\mathcal{X}} \cap \mathcal{G}$, respectively detect emptiness of this intersection, in low dimensions. The key idea is to exploit that $\widehat{\mathcal{X}}$ is decomposed. For ease of discussion, we consider the case of two blocks (i.e., $\widehat{\mathcal{X}} = \mathcal{X}_1 \times \mathcal{X}_2$). Below we discuss the two cases that \mathcal{G} is decomposed or not.

Intersection between two decomposed sets. We first consider the case that \mathcal{G} is also decomposed and agrees with $\widehat{\mathcal{X}}$ on the block structure, i.e., $\mathcal{G} = \widehat{\mathcal{G}} = \mathcal{G}_1 \times \mathcal{G}_2$ and $\mathcal{X}_1, \mathcal{G}_1 \subseteq \mathbb{R}^{n_1}$ for some n_1 . Clearly

$$\widehat{\mathcal{X}} \cap \widehat{\mathcal{G}} = (\mathcal{X}_1 \times \mathcal{X}_2) \cap (\mathcal{G}_1 \times \mathcal{G}_2) = (\mathcal{X}_1 \cap \mathcal{G}_1) \times (\mathcal{X}_2 \cap \mathcal{G}_2)$$

because the Cartesian product and intersection distribute, and thus

$$\widehat{\mathcal{X}} \cap \widehat{\mathcal{G}} = \emptyset \iff (\mathcal{X}_1 \cap \mathcal{G}_1 = \emptyset) \vee (\mathcal{X}_2 \cap \mathcal{G}_2 = \emptyset). \quad (5)$$

Now consider the second disjunct in (5) and assume that \mathcal{G}_2 is universal. We get $\mathcal{X}_2 \cap \mathcal{G}_2 = \emptyset \iff \mathcal{X}_2 = \emptyset$. In our context, $\widehat{\mathcal{X}}$ (and hence \mathcal{X}_2) is nonempty by construction. Hence (5) simplifies to

$$\widehat{\mathcal{X}} \cap \widehat{\mathcal{G}} = \emptyset \iff \mathcal{X}_1 \cap \mathcal{G}_1 = \emptyset,$$

so we *never* need to compute \mathcal{X}_2 to determine whether the intersection is empty. In practice, the set \mathcal{G}^* from (4) takes the role of $\widehat{\mathcal{G}}$ and is often only constrained in *some* dimensions (and hence decomposed and universal in all other dimensions).

Intersection between a decomposed and a non-decomposed set. In general, if \mathcal{G} is not decomposed in the same block structure as \mathcal{X} , we can still decompose it, at the cost of an approximation error. Let π_i be suitable projection matrices. Then

$$\widehat{\mathcal{X}} \cap \mathcal{G} \subseteq (\mathcal{X}_1 \cap \pi_1 \mathcal{G}) \times (\mathcal{X}_2 \cap \pi_2 \mathcal{G})$$

and hence

$$\begin{aligned} \widehat{\mathcal{X}} \cap \mathcal{G} = \emptyset &\iff (\mathcal{X}_1 \cap \pi_1 \mathcal{G} = \emptyset) \vee (\mathcal{X}_2 \cap \pi_2 \mathcal{G} = \emptyset) \\ &\iff \mathcal{X}_1 \cap \pi_1 \mathcal{G} = \emptyset. \end{aligned} \quad (6)$$

From (6) we obtain (1) a sufficient test for emptiness of $\widehat{\mathcal{X}} \cap \mathcal{G}$ in terms of only \mathcal{X}_1 and (2) a more precise sufficient test in terms of \mathcal{X}_1 and \mathcal{X}_2 in low dimensions. If both tests fail, we can either fall back to the (exact) test in high dimensions or conservatively assume that the intersection is nonempty.

The precision of the above scheme highly depends on the structure of $\widehat{\mathcal{X}}$ and \mathcal{G} . If several (but not all) blocks of \mathcal{G} are constrained, instead of decomposing \mathcal{G} into the low-dimensional block structure, one can alternatively compute the intersection for medium-dimensional sets to avoid an approximation error; we apply this strategy in the evaluation (Section 5). If \mathcal{G} is compact, the following proposition shows that the approximation error is bounded by the maximal entry in the diameters of $\widehat{\mathcal{X}}$ and \mathcal{G} , and this bound is tight.

PROPOSITION 4.1. *Let $\widehat{\mathcal{X}} = \times_j \mathcal{X}_j \in \mathcal{C}_n$, $\mathcal{G} \in \mathcal{C}_n$, $\widehat{\mathcal{X}} \cap \mathcal{G} \neq \emptyset$, $\widehat{\mathcal{G}} := \times_j \pi_j \mathcal{G}$ for appropriate projection matrices π_j corresponding to \mathcal{X}_j , and $p = \infty$. Then*

$$d_H^p(\widehat{\mathcal{X}} \cap \mathcal{G}, \widehat{\mathcal{X}} \cap \widehat{\mathcal{G}}) \leq \max_j \min(\|\Delta_p(\mathcal{X}_j)\|_p, \|\Delta_p(\pi_j \mathcal{G})\|_p).$$

Example. Consider again Figure 5. We have already identified the intersection with the flowpipe for time steps $k = 3$ and $k = 4$. The resulting sets are $\widehat{\mathcal{X}}(k) \cap \mathcal{G} = \mathcal{X}_1(k) \cap \mathcal{G}_1 \times \mathcal{X}_2(k)$, where \mathcal{G}_1 was the projection of \mathcal{G} to x_1 . We emphasize that we compute the intersections in low dimensions, that we need not compute $\mathcal{X}_2(1)$ and $\mathcal{X}_2(2)$ at all, and that in this example all computations are exact (i.e., we obtain the same sets as in Figure 3).

Now consider the case that \mathcal{G} is not decomposed in the same structure as $\widehat{\mathcal{X}}$, e.g., the hyperplane $x_1 = x_2$. One option is to decompose \mathcal{G} to the blocks of $\widehat{\mathcal{X}}$, i.e., $\mathcal{G}_1 := \pi_1 \mathcal{G}$, $\mathcal{G}_2 := \pi_2 \mathcal{G}$ and compute the block-wise intersection $(\mathcal{X}_1(k) \cap \mathcal{G}_1) \times (\mathcal{X}_2(k) \cap \mathcal{G}_2)$. Here \mathcal{G}_1 and \mathcal{G}_2 are universal, so we obtain a coarse approximation of the intersection (namely $\widehat{\mathcal{X}}(k)$ itself). Alternatively, computing the intersection $\widehat{\mathcal{X}}(k) \cap \mathcal{G}$ is exact but computationally more demanding. If we assume that the system has higher dimension, e.g., 10, then computing the intersection in two dimensions (i.e., with a 2D projection $\widehat{\mathcal{X}}(k) \cap \pi \mathcal{G}$) is still exact and yet cheaper than computing the intersection in full dimensions (i.e., $(\widehat{\mathcal{X}}(k) \times \text{Univ}_8) \cap \mathcal{G}$, where Univ_8 is the eight-dimensional universe).

Remark 1. Computing the intersection of two n -dimensional sets \mathcal{X} and \mathcal{G} in low dimensions is generally beneficial for performance; yet it is particularly interesting if one of the sets is a polytope that is not represented by its constraints. Common cases are the vertex representation or zonotopes

represented by their generators, which are used in several approaches [4, 6, 25, 27]. To compute the (exact) intersection of such a polytope \mathcal{X} with a polyhedron \mathcal{G} in constraint representation, \mathcal{X} needs to be converted to constraint representation first. A polytope with m vertices can have $O\left(\binom{m-n/2}{m-n}\right)$ constraints [40]. (For two polytopes in vertex representation *in general position* there is a polynomial-time intersection algorithm [24], but this assumption is not practical.) A zonotope with m generators can have $O(m \binom{m}{n-1})$ constraints [6]. If \mathcal{G} is a polytope in constraint representation, checking disjointness of \mathcal{X} and \mathcal{G} can also be solved more efficiently in low dimensions, e.g., for m constraints in $O(m)$ for $n \leq 3$ [10].

4.3 Decomposing an affine map

The next step after computing the intersection with the guard is the application of the assignment. We consider an affine map $A\widehat{\mathcal{X}} \oplus \{b\}$ with $A \in \mathbb{R}^{n \times n}$ and $b \in \mathbb{R}^n$. Affine-map decomposition has already been presented as part of the operator Post_C^\square [11]:

$$A\widehat{\mathcal{X}} \oplus \{b\} \subseteq \times_i \bigoplus_j A_{ij} \mathcal{X}_j \oplus \{b_i\}$$

where A_{ij} is the block in the i -th block row and the j -th block column. We recall an error estimation.

PROPOSITION 4.2. [11, Prop. 3] *Let $\mathcal{X} = \times_{j=1}^\beta \mathcal{X}_j \in \mathcal{C}_n$ be nonempty, $A \in \mathbb{R}^{n \times n}$, $q_j := \arg \max_i \|A_{ij}\|_p$ (the index of the block with the largest matrix norm in the j -th block column) so that $\alpha_j := \max_{i \neq q_j} \|A_{ij}\|_p$ is the second largest matrix norm in the j -th block column. Let $\alpha_{\max} := \max_j \alpha_j$ and $\Delta_{\text{sum}} := \sum_j \Delta_\infty(\mathcal{X}_j)$. Then*

$$\begin{aligned} d_H^p(A\mathcal{X}, \times_i \bigoplus_j A_{ij} \mathcal{X}_j) \\ &= \max_{\|d\|_p \leq 1} \sum_{i,j} \rho_{\mathcal{X}_j}(A_{ij}^T d_i) - \rho_{\mathcal{X}_j} \left(\sum_k A_{kj}^T d_k \right) \\ &\leq (\beta - 1) \sum_j \alpha_j \Delta_\infty(\mathcal{X}_j) \leq \frac{n}{2} \alpha_{\max} \Delta_{\text{sum}}. \end{aligned}$$

In particular, if only one block per block column of matrix A is nonzero, the approximation is exact [11]. For example, consider a two-block scenario and a block-diagonal matrix A , i.e., $A_{12} = A_{21} = 0$. Then

$$\begin{aligned} \begin{pmatrix} A_{11} & 0 \\ 0 & A_{22} \end{pmatrix} \mathcal{X}_1 \times \mathcal{X}_2 \oplus \{b_1\} \times \{b_2\} \\ = (A_{11} \mathcal{X}_1 \oplus \{b_1\}) \times (A_{22} \mathcal{X}_2 \oplus \{b_2\}). \end{aligned}$$

In practice, affine maps with such a structure are unrealistic for the Post_C^\square operator but typical for assignments. Prominent cases include resets, translations, and scalings, for which A is even diagonal and hence block diagonal for any block structure.

Example. Recall that, after computing the intersections, we ended up with the same sets as in Figure 3. In our example, the assignment is a translation in dimension x_1 . Hence, as mentioned above, the application of the decomposed assignment is also exact. In particular, the translation only affects $\mathcal{X}_1(k)$. Thus we again obtain the same result as in Figure 3.

4.4 Inclusion check for decomposed sets

Our algorithm is now fully able to take transitions. Observe that *all* sets ever occurring in scheme (3) using the algorithm are decomposed. The following proposition gives an exact low-dimensional fixpoint check under this condition.

PROPOSITION 4.3. *Let $\widehat{\mathcal{X}} = \times_j \mathcal{X}_j \in \mathcal{C}_n$, $\widehat{\mathcal{G}} = \times_j \mathcal{G}_j \in \mathcal{C}_n$ be nonempty sets with identical block structure. Then*

$$\widehat{\mathcal{X}} \subseteq \widehat{\mathcal{G}} \iff \bigwedge_j \mathcal{X}_j \subseteq \mathcal{G}_j.$$

4.5 Decomposing a convex hull

As the last part of the algorithm, we decompose the computation of the convex hull. We exploit that all sets in the same flowpipe share the same block structure.

PROPOSITION 4.4. *Let $\widehat{\mathcal{X}} = \times_j \mathcal{X}_j \in \mathcal{C}_n$, $\widehat{\mathcal{G}} = \times_j \mathcal{G}_j \in \mathcal{C}_n$ be nonempty sets with identical block structure. Then*

$$\text{CH}(\widehat{\mathcal{X}} \cup \widehat{\mathcal{G}}) \subseteq \times_j \text{CH}(\mathcal{X}_j \cup \mathcal{G}_j).$$

For the decomposition operations proposed before (intersection, affine map, and inclusion), there are common cases where the approximations were exact. In these cases it is always beneficial to perform the decomposed operations instead of the high-dimensional counterparts. The decomposition of the convex hull, however, always incurs an approximation error, which we can bound by the radius of the box approximation and by the block-wise difference in bounds.

PROPOSITION 4.5. *Let $\widehat{\mathcal{X}} = \times_j \mathcal{X}_j \in \mathcal{C}_n$, $\widehat{\mathcal{G}} = \times_j \mathcal{G}_j \in \mathcal{C}_n$ be nonempty sets with identical block structure and let r^∞ be the radius of the box approximation of $\text{CH}(\widehat{\mathcal{X}} \cup \widehat{\mathcal{G}})$. Then*

$$\begin{aligned} & d_H^p(\text{CH}(\widehat{\mathcal{X}} \cup \widehat{\mathcal{G}}), \times_j \text{CH}(\mathcal{X}_j \cup \mathcal{G}_j)) \\ & \leq \min \left(\|r^\infty\|_\infty, \max_{\|d\|_p \leq 1} \sum_j |\rho_{\mathcal{X}_j}(d_j) - \rho_{\mathcal{G}_j}(d_j)| \right). \end{aligned}$$

Example. Figure 4 shows the decomposed convex hull of the sets $\widehat{\mathcal{X}}(3) \cap \mathcal{G}$ and $\widehat{\mathcal{X}}(4) \cap \mathcal{G}$ after applying the translation. Since each block is one-dimensional in our example, we obtain the box approximation.

5 EVALUATION

We implemented the ideas presented in Section 4 in JuliaReach [2, 12]. The code is publicly available [2]. We performed the experiments presented in this section on a Mac notebook with an Intel i5 CPU@3.1 GHz and 16 GB RAM.

5.1 Benchmark descriptions

We evaluate our implementation on a number of benchmarks taken from the HyPro model library [1], from the ARCH-COMP 2019 competition [3], and a scalable model from [21]. To demonstrate the qualitative performance of our approach, we verify a safety property for each benchmark, which requires precise approximations in each step of the algorithm. We briefly describe the benchmarks below.

Linear switching system. This five-dimensional model taken from [1] is a piecewise-linear system with five locations of different controlled, randomly-generated continuous dynamics stabilized by an LQR controller. The hybrid system has a ring topology whose transitions are determined heuristically from simulations. The safety property for this system is $x_1 > -1.2$.

Spacecraft rendezvous. This model with five dimensions represents a spacecraft steering toward a passive target in space [15]. We use a linearized version of this model with three locations. We consider two scenarios, one where the spacecraft successfully approaches the target and another one where a mission abort occurs at $t = 120$ min. For the safety properties we refer to [3].

Platooning. This ten-dimensional model with two locations represents a platoon of three vehicles with communication loss at deterministic times [39]. The safety property enforces a minimum distance d between the vehicles: $\bigwedge_{x \in \{x_1, x_4, x_7\}} x \geq -d$. We consider both a time-bounded setting with $d = 42$ and a time-unbounded setting with $d = 50$; note that in the latter setting a fixpoint must be found.

Filtered oscillator. This model consists of a two-dimensional switched oscillator (dimensions x and y) and a parametric number of filters (here: 64–1024) which smooth x [21]. We fixed the maximum number of transitions to five by adding a new variable. The safety property is $y < 0.5$.

5.2 Tool descriptions

We compare our implementation in JuliaReach to two other algorithms available in the same tool. All three algorithms use the same decomposition-based continuous-post operator Post_C^\square [12], so the main difference between these algorithms is the intersection operation with discrete jumps, which allows for a direct comparison of the approach presented in this paper. Furthermore, we compare the implementation to two algorithms available in SpaceEx [21], which is an efficient and mature verification tool for linear hybrid systems. We shortly summarize these different approaches below.

Deco. This algorithm implements the approach presented in this paper. To compute the (low-dimensional) intersections, we use a polyhedra library [38].

LazySupp. This algorithm uses a (lazy) support-function-based approximation of the intersection operation using the

Table 1. For each benchmark we report the number of dimension n and the number of constrained dimensions (*Dim. (constr.)*), the step size of the time discretization (*Step*) and the runtime of the different algorithms in seconds (where the fastest solution is marked in bold face). For benchmark instances with underlined computation time, the safety property was not satisfied, in which case the computation terminated as soon as the violation was detected. “TO” and “OOM” indicate a timeout of 5×10^4 seconds and an out-of-memory error, respectively.

Benchmark	Dim. (constr.)	Step	Deco	LazySupp	LazyOptim	SpaceEx LGG	SpaceEx STC
linear_switching	5 (1)	0.0001	2.50×10^0	1.27×10^1	2.81×10^1	2.60×10^1	2.30×10^1
spacecraft_noabort	5 (4)	0.04	5.30×10^0	3.42×10^0	2.19×10^2	1.18×10^0	3.50×10^{-1}
spacecraft_120	5 (5)	0.04	5.30×10^0	2.10×10^0	4.30×10^1	1.91×10^0	8.10×10^{-1}
platoon_bounded	10 (4)	0.01	1.30×10^{-1}	1.60×10^{-1}	5.69×10^0	5.55×10^0	1.60×10^0
platoon_unbounded	10 (4)	0.03	1.08×10^0	1.16×10^0	4.96×10^1	3.46×10^1	6.50×10^1
filtered_osc64	67 (3)	0.01	2.81×10^0	<u>7.43×10^0</u>	5.63×10^3	2.04×10^1	3.25×10^1
filtered_osc128	131 (3)	0.01	7.95×10^0	<u>4.29×10^1</u>	1.79×10^3	1.69×10^2	4.67×10^4
filtered_osc256	259 (3)	0.01	2.80×10^1	<u>9.19×10^1</u>	9.99×10^4	8.70×10^3	OOM
filtered_osc512	515 (3)	0.01	1.13×10^2	<u>4.73×10^3</u>	TO	TO	TO
filtered_osc1024	1027 (3)	0.01	5.09×10^2	<u>5.11×10^3</u>	TO	TO	TO

simple heuristics $\rho_{X \cap Y}(\ell) \leq \min(\rho_X(\ell), \rho_Y(\ell))$. This heuristics is fast but not precise enough to verify the safety property of the *filtered oscillator* model.

LazyOptim. In contrast to the coarse intersection in LazySupp, this algorithm uses a more precise implementation of the intersection operation based on line search [23].

SpaceEx LGG. This is an efficient implementation of the algorithm by Le Guernic and Girard [30].

SpaceEx STC. The STC algorithm is an extension of the LGG algorithm with automatic time-step adaptation [22].

All tools use a support-function representation of sets and we use template polyhedra with box constraints to overapproximate those sets, which roughly corresponds to a decomposition into one-dimensional blocks and is fast. For the algorithms implemented in JuliaReach, we use one-dimensional block structures for all models. For SpaceEx we use the options given in the benchmark sources. For algorithms that use a fixed time step, we fix this parameter to the same value for each benchmark. The SpaceEx STC algorithm does not have a time-step parameter, so we instead fix the parameter “flowpipe tolerance”, which controls the approximation error, to the following values: *linear switching system*: 0.01, *spacecraft*: 0.2, *platooning*: 1, *filtered oscillator*: 0.05.

5.3 Experimental results

The results are presented in Table 1. We generally observe a performance boost of the Deco algorithm for models with more than five dimensions, and only a minor overhead for “small” models. This demonstrates the general scalability improvement by performing operations, especially the intersection, in low dimensions. Since all models have a small

Table 2. Evaluation for different time steps on the *filtered oscillator* model with 64 filters (“filtered_osc64” in Table 1). We compare all algorithms that allow to vary the time step. The last row shows the relative change of the fourth row with the first row as base line.

Step	Deco	LazySupp	LazyOptim	SpaceEx LGG
0.01	2.8×10^0	7.4×10^0	5.6×10^2	2.0×10^1
0.005	4.1×10^0	1.3×10^1	9.5×10^2	3.6×10^1
0.001	1.7×10^1	6.5×10^1	4.7×10^3	1.6×10^2
0.0005	3.2×10^1	1.3×10^2	8.4×10^3	3.2×10^2
$\times 20.0$	$\times 11.4$	$\times 17.5$	$\times 15.0$	$\times 16.0$

number of constrained dimensions in their guards and invariants, choosing an appropriate block structure results in very low-dimensional sets for computing the intersections, for which concrete polyhedral computations are very efficient and most precise. We note that such an intersection computation does not scale with the dimension, and so other algorithms must resort to approximation techniques.

Moreover, we found that our approach scales more favorably compared to the high-dimensional approaches when decreasing the time step δ (cf. Section 3.1). We demonstrate this observation for the *filtered oscillator* model in Table 2 and explain it as follows. Recall that we only compute those sets in the flowpipe in high dimensions for which we have detected an intersection in low dimensions. With a smaller time step, the total number of sets increases and hence the savings due to our approach become more dominant. To give an example, for the *filtered oscillator* with time step 0.0005, out of the 9,661 sets in total we only computed 1,400 sets in high dimensions.

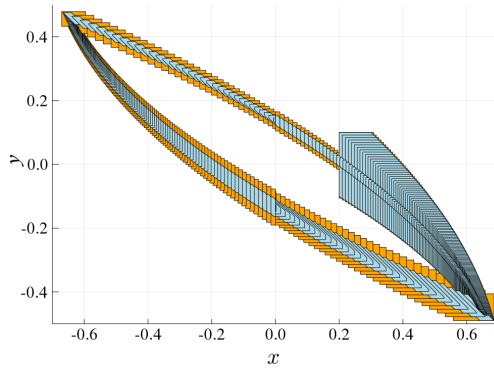


Figure 6. Two flowpipes for the model *filtered oscillator*. The blue flowpipe is obtained with two-dimensional block structure and octagon approximation, and the orange flowpipe is obtained with one-dimensional block structure. In both cases the time step is 0.01.

Furthermore, while in general our algorithm may induce an additional approximation error with the block structure, in the evaluation it was always precise enough to prove safety. In the Table 1 we report the total amount of constrained dimensions in guards, invariants, and safety properties for each benchmark instance. These are the dimensions that determine our low-dimensional flowpipes. For some of the models, the constrained dimensions differ between the invariants/guards and the safety property, but a one-dimensional block structure was still sufficient. Note that we need to compute intersections only with invariants and guards; for safety properties we just need to check inclusion.

In the *linear switching* model, only one dimension is constrained, so our algorithm, together with one-dimensional block structure, is appropriate, especially because a small time step is required to satisfy the property. In the *platooning* model, the safety property constrains three dimensions but the invariants and guards constrain just one dimension.

The invariants and guards of the models *spacecraft* and *filtered oscillator* constrain two dimensions, so the natural choice for the decomposition is to keep these dimensions in the same block. However, we chose to decompose into one-dimensional blocks for better runtime comparison in Table 1. In the implementation, we follow the strategy to perform the intersection in two dimensions and then project back to one dimension (cf. Section 4.2). If instead we decide to employ a two-dimensional block structure, we can further gain precision by using different template polyhedra, e.g., with octagon constraints. In Figure 6 we visualize this alternative for the *filtered oscillator*. As expected, the one-dimensional analysis is less precise as it corresponds to a box overapproximation. However, we note that a one-dimensional block structure also inherently reduces the precision of $Post_C^\square$, so

the additional approximation error does not only stem from the discrete transitions due to our approach.

6 CONCLUSION

We have presented a schema that integrates a reachability algorithm based on decomposition for LTI systems in the analysis loop for linear hybrid systems. The key insight is that intersections with polyhedral constraints can be efficiently detected and computed (approximately or often even exactly) in low dimensions. This enables the systematic focus on appropriate subspaces and the potential for bypassing large amounts of flowpipe computations. Moreover, working with sets in low dimensions allows to use precise polyhedral computations that are infeasible in high dimensions.

Future work. An essential step in our algorithm is the fast computation of a low-dimensional flowpipe for the detection of intersections. In the presented algorithm, we recompute the flowpipe for the relevant time frames in high dimensions using the same decomposed algorithm with the same time step. However, this is not necessary. We could achieve higher precision by using different algorithmic parameters or even a different, possibly non-decomposed, algorithm (e.g., one that features arbitrary precision [26]). This is particularly promising for LTI systems because one can avoid recomputing the homogeneous (state-based) part of the flowpipe [23].

In the benchmarks considered in the experimental evaluation, it was not necessary to change the block structure when switching between locations. In general, different locations may constrain different dimensions, so tracking the “right” dimensions may be necessary to maintain precision. While it is easy to merge different blocks, subsequent computations would become more expensive. Hence one may also want to split blocks again for optimal performance. Since this comes with a loss in precision, heuristics for rearranging the block structure, possibly in a refinement loop, are needed.

ACKNOWLEDGEMENTS

This research was supported in part by the Austrian Science Fund (FWF) under grants S11402-N23 (RiSE/SHiNE) and Z211-N23 (Wittgenstein Award), the European Union’s Horizon 2020 research and innovation programme under the Marie Skłodowska-Curie grant agreement No. 754411, and the Air Force Office of Scientific Research under award number FA2386-17-1-4065. Any opinions, findings, and conclusions or recommendations expressed in this material are those of the authors and do not necessarily reflect the views of the United States Air Force.

REFERENCES

- [1] 2019. HyPro Benchmark Repository. <https://ths.rwth-aachen.de/research/projects/hypro/benchmarks-of-continuous-and-hybrid-systems/>.
- [2] 2019. JuliaReach. <https://github.com/JuliaReach>.
- [3] Matthias Althoff, Stanley Bak, Marcelo Forets, Goran Frehse, Niklas Kochdumper, Rajarshi Ray, Christian Schilling, and Stefan Schupp. 2019. ARCH-COMP19 Category Report: Continuous and Hybrid Systems with Linear Continuous Dynamics. *EPiC Series in Computing* 61 (2019), 14–40.
- [4] Matthias Althoff and Goran Frehse. 2016. Combining zonotopes and support functions for efficient reachability analysis of linear systems. In *CDC*. 7439–7446. <https://doi.org/10.1109/CDC.2016.7799418>
- [5] Matthias Althoff and Bruce H. Krogh. 2012. Avoiding geometric intersection operations in reachability analysis of hybrid systems. In *HSCC*. 45–54. <https://doi.org/10.1145/2185632.2185643>
- [6] Matthias Althoff, Olaf Stursberg, and Martin Buss. 2010. Computing reachable sets of hybrid systems using a combination of zonotopes and polytopes. *Nonlinear Analysis: Hybrid Systems* 2 (2010), 233–249. <https://doi.org/10.1016/j.nahs.2009.03.009>
- [7] Rajeev Alur, Costas Courcoubetis, Thomas A. Henzinger, and Pei-Hsin Ho. 1992. Hybrid Automata: An Algorithmic Approach to the Specification and Verification of Hybrid Systems. In *Hybrid Systems*. 209–229. https://doi.org/10.1007/3-540-57318-6_30
- [8] Eugene Asarin and Thao Dang. 2004. Abstraction by Projection and Application to Multi-affine Systems. In *HSCC*. https://doi.org/10.1007/978-3-540-24743-2_3
- [9] Stanley Bak, Sergiy Bogomolov, and Matthias Althoff. 2017. Time-Triggered Conversion of Guards for Reachability Analysis of Hybrid Automata. In *FORMATS*. 133–150. https://doi.org/10.1007/978-3-319-65765-3_8
- [10] Luis Barba and Stefan Langerman. 2015. Optimal detection of intersections between convex polyhedra. In *SODA*. <https://doi.org/10.1137/1.9781611973730.109>
- [11] Sergiy Bogomolov, Marcelo Forets, Goran Frehse, Andreas Podelski, Christian Schilling, and Frédéric Viry. 2018. Reach Set Approximation through Decomposition with Low-dimensional Sets and High-dimensional Matrices. In *HSCC*. 41–50. <https://doi.org/10.1145/3178126.3178128>
- [12] Sergiy Bogomolov, Marcelo Forets, Goran Frehse, Kostiantyn Potomkin, and Christian Schilling. 2019. JuliaReach: a Toolbox for Set-Based Reachability. In *HSCC*. <https://doi.org/10.1145/3302504.3311804>
- [13] Sergiy Bogomolov, Goran Frehse, Mirco Giacobbe, and Thomas A. Henzinger. 2017. Counterexample-guided refinement of template polyhedra. In *TACAS*. 589–606. https://doi.org/10.1007/978-3-662-54577-5_34
- [14] Lei Bu and Xuandong Li. 2011. Path-oriented bounded reachability analysis of composed linear hybrid systems. *STTT* 4 (2011), 307–317. <https://doi.org/10.1007/s10009-010-0163-9>
- [15] Nicole Chan and Sayan Mitra. 2017. Verifying safety of an autonomous spacecraft rendezvous mission. In *ARCH*. <http://www.easychair.org/publications/paper/342723>
- [16] Mo Chen, Sylvia L. Herbert, and Claire J. Tomlin. 2017. Exact and efficient Hamilton-Jacobi guaranteed safety analysis via system decomposition. In *ICRA*. 87–92. <https://doi.org/10.1109/ICRA.2017.7989015>
- [17] Xin Chen and Sriram Sankaranarayanan. 2016. Decomposed Reachability Analysis for Nonlinear Systems. In *RTSS*. 13–24. <https://doi.org/10.1109/RTSS.2016.011>
- [18] Alongkritt Chutinan and Bruce H. Krogh. 2003. Computational techniques for hybrid system verification. *IEEE Trans. Automat. Contr.* 1 (2003), 64–75. <https://doi.org/10.1109/TAC.2002.806655>
- [19] Asen L. Dontchev. 1992. Time-scale decomposition of the reachable set of constrained linear systems. *MCSS* 3 (1992), 327–340. <https://doi.org/10.1007/BF01211565>
- [20] Goran Frehse, Sergiy Bogomolov, Marius Greitschus, Thomas Strump, and Andreas Podelski. 2015. Eliminating spurious transitions in reachability with support functions. In *HSCC*. 149–158. <http://doi.acm.org/10.1145/2728606.2728622>
- [21] Goran Frehse, Colas Le Guernic, Alexandre Donzé, Scott Cotton, Rajarshi Ray, Olivier Lebeltel, Rodolfo Ripado, Antoine Girard, Thao Dang, and Oded Maler. 2011. SpaceEx: Scalable Verification of Hybrid Systems. In *CAV*. 379–395. https://doi.org/10.1007/978-3-642-22110-1_30
- [22] Goran Frehse, Rajat Kateja, and Colas Le Guernic. 2013. Flowpipe approximation and clustering in space-time. In *HSCC*. 203–212. <https://doi.org/10.1145/2461328.2461361>
- [23] Goran Frehse and Rajarshi Ray. 2012. Flowpipe-Guard Intersection for Reachability Computations with Support Functions. In *ADHS*. 94–101. <https://doi.org/10.3182/20120606-3-NL-3011.00053>
- [24] Komei Fukuda, Thomas M. Liebling, and Christine Lütolf. 2001. Extended convex hull. *Comput. Geom.* 1-2 (2001), 13–23. [https://doi.org/10.1016/S0925-7721\(01\)00032-3](https://doi.org/10.1016/S0925-7721(01)00032-3)
- [25] Antoine Girard. 2005. Reachability of Uncertain Linear Systems Using Zonotopes. In *HSCC*. 291–305. https://doi.org/10.1007/978-3-540-31954-2_19
- [26] Antoine Girard and Colas Le Guernic. 2008. Efficient reachability analysis for linear systems using support functions. *IFAC Proceedings Volumes* 2 (2008), 8966–8971. <https://doi.org/10.3182/20080706-5-KR-1001.01514>
- [27] Antoine Girard and Colas Le Guernic. 2008. Zonotope/Hyperplane Intersection for Hybrid Systems Reachability Analysis. In *HSCC*. 215–228. https://doi.org/10.1007/978-3-540-78929-1_16
- [28] Elena V. Goncharova and Alexander I. Ovseevich. 2009. Asymptotics for Singularly Perturbed Reachable Sets. In *LSSC*. 280–285. https://doi.org/10.1007/978-3-642-12535-5_32
- [29] Mark R. Greenstreet and Ian Mitchell. 1999. Reachability Analysis Using Polygonal Projections. In *HSCC*. 103–116. https://doi.org/10.1007/3-540-48983-5_12
- [30] Colas Le Guernic and Antoine Girard. 2009. Reachability Analysis of Hybrid Systems Using Support Functions. In *CAV*. 540–554. https://doi.org/10.1007/978-3-642-02658-4_40
- [31] Abdullah Omar Hamadeh and Jorge M. Goncalves. 2008. Reachability analysis of continuous-time piecewise affine systems. *Automatica* 12 (2008), 3189–3194. <https://doi.org/10.1016/j.automatica.2008.05.023>
- [32] Zhi Han and Bruce H. Krogh. 2006. Reachability Analysis of Large-Scale Affine Systems Using Low-Dimensional Polytopes. In *HSCC*. 287–301. https://doi.org/10.1007/11730637_23
- [33] Thomas A. Henzinger. 1996. The Theory of Hybrid Automata. In *LICS*. 278–292. <https://doi.org/10.1109/LICS.1996.561342>
- [34] Dorit S. Hochbaum and Joseph Naor. 1994. Simple and Fast Algorithms for Linear and Integer Programs With Two Variables per Inequality. *SIAM J. Comput.* 6 (1994), 1179–1192. <https://doi.org/10.1137/S0097539793251876>
- [35] Shahab Kaynama and Meeko Oishi. 2010. Overapproximating the reachable sets of LTI systems through a similarity transformation. In *ACC*. 1874–1879. <https://doi.org/10.1109/ACC.2010.5531392>
- [36] Shahab Kaynama and Meeko Oishi. 2011. Complexity reduction through a Schur-based decomposition for reachability analysis of linear time-invariant systems. *Int. J. Control* 1 (2011), 165–179. <https://doi.org/10.1080/00207179.2010.543703>
- [37] Colas Le Guernic. 2009. *Reachability analysis of hybrid systems with linear continuous dynamics*. Ph.D. Dissertation. Université Grenoble 1 - Joseph Fourier. <https://tel.archives-ouvertes.fr/tel-00422569>

- [38] Benoît Legat, Robin Deits, Oliver Evans, Gustavo Goretkin, Twan Koolen, Joey Huchette, Daisuke Oyama, Marcelo Forets, guberger, Robert Schwarz, Henrique Ferrolho, Elliot Saba, and Chase Coleman. 2019. *JuliaPolyhedra/Polyhedra.jl: v0.5.6*. <https://doi.org/10.5281/zenodo.3454699>
- [39] Ibtissem Ben Makhlof and Stefan Kowalewski. 2014. Networked Cooperative Platoon of Vehicles for Testing Methods and Verification Tools. In *ARCH*. 37–42. <http://www.easychair.org/publications/paper/252253>
- [40] Peter McMullen. 1970. The maximal number of faces of a convex polytope. *Mathematika* (1970), 179–184.
- [41] Ian M. Mitchell and Claire Tomlin. 2003. Overapproximating Reachable Sets by Hamilton-Jacobi Projections. *J. Sci. Comput.* 1-3 (2003), 323–346. <https://doi.org/10.1023/A:1025364227563>
- [42] Nediako S. Nediakov and Martin Von Mohrenschildt. 2002. Rigorous simulation of hybrid dynamic systems with symbolic and interval methods. In *ACC*. 140–147. <https://doi.org/10.1109/ACC.2002.1024794>
- [43] Stefan Schupp, Johanna Nellen, and Erika Ábrahám. 2017. Divide and Conquer: Variable Set Separation in Hybrid Systems Reachability Analysis. In *QAPL@ETAPS*. 1–14. <https://doi.org/10.4204/EPTCS.250.1>
- [44] Yassamine Seladji and Olivier Bouissou. 2013. Numerical Abstract Domain Using Support Functions. In *NASA Formal Methods*. 155–169. https://doi.org/10.1007/978-3-642-38088-4_11
- [45] Chao Yan and Mark R. Greenstreet. 2008. Faster projection based methods for circuit level verification. In *ASP-DAC*. 410–415. <https://doi.org/10.1109/ASPDAC.2008.4483985>

A PROOFS

PROPOSITION 2.1. Recall that

$$d_H^p(\mathcal{X}, \times_j \pi_j \mathcal{X}) = \inf_{\varepsilon \in \mathbb{R}} \left\{ \times_j \pi_j \mathcal{X} \subseteq \mathcal{X} \oplus \varepsilon \mathcal{B}_p^n \text{ and } \mathcal{X} \subseteq \times_j \pi_j \mathcal{X} \oplus \varepsilon \mathcal{B}_p^n \right\}.$$

We claim that $\|r_{\mathcal{X}}^p\|_p$ is an upper bound on ε , which we now prove by showing the two inclusions. One inclusion is trivial because $\mathcal{X} \subseteq \times_j \pi_j \mathcal{X}$. For the other inclusion, observe that the center of the box approximation of \mathcal{X} , $c_{\mathcal{X}}^p$, lies in \mathcal{X} . Recall that $p = \infty$ and that the box approximation of \mathcal{X} , $\{c_{\mathcal{X}}^p\} \oplus \|r_{\mathcal{X}}^p\|_p \mathcal{B}_p^n$, is the worst-case decomposition of \mathcal{X} , subsuming all other decompositions.

$$\times_j \pi_j \mathcal{X} \subseteq \{c_{\mathcal{X}}^p\} \oplus \|r_{\mathcal{X}}^p\|_p \mathcal{B}_p^n \subseteq \mathcal{X} \oplus \|r_{\mathcal{X}}^p\|_p \mathcal{B}_p^n \quad \square$$

PROPOSITION 4.1.

$$\begin{aligned} & d_H^p(\widehat{\mathcal{X}} \cap \widehat{\mathcal{G}}, \widehat{\mathcal{X}} \cap \widehat{\mathcal{G}}) \\ &= \max_{\|d\|_p \leq 1} \rho_{\widehat{\mathcal{X}} \cap \widehat{\mathcal{G}}}(d) - \rho_{\widehat{\mathcal{X}} \cap \widehat{\mathcal{G}}}(d) \\ &= \max_{\|d\|_p \leq 1} \max_{x \in \widehat{\mathcal{X}} \cap \widehat{\mathcal{G}}} \langle d, x \rangle - \max_{y \in \widehat{\mathcal{X}} \cap \widehat{\mathcal{G}}} \langle d, y \rangle \\ &= \max_{\|d\|_p \leq 1} \max_{x \in \widehat{\mathcal{X}} \cap \widehat{\mathcal{G}}} \min_{y \in \widehat{\mathcal{X}} \cap \widehat{\mathcal{G}}} \langle d, x - y \rangle \end{aligned}$$

We can take absolute values in the dot product by choosing d accordingly.

$$\begin{aligned} &= \max_{\|d\|_p \leq 1} \max_{x \in \widehat{\mathcal{X}} \cap \widehat{\mathcal{G}}} \min_{y \in \widehat{\mathcal{X}} \cap \widehat{\mathcal{G}}} \langle d, |x - y| \rangle \\ &\leq \max_{\|d\|_p \leq 1} \max_{x, y \in \widehat{\mathcal{X}} \cap \widehat{\mathcal{G}}} \langle d, |x - y| \rangle \end{aligned}$$

We can conservatively bound the distance $|x - y|$ by the diameter of $\widehat{\mathcal{X}} \cap \widehat{\mathcal{G}}$.

$$\begin{aligned} &\leq \max_{\|d\|_p \leq 1} \langle d, \Delta_p(\widehat{\mathcal{X}} \cap \widehat{\mathcal{G}}) \rangle \\ &\leq \min \left(\max_{\|d\|_p \leq 1} \langle d, \Delta_p(\widehat{\mathcal{X}}) \rangle, \max_{\|d\|_p \leq 1} \langle d, \Delta_p(\widehat{\mathcal{G}}) \rangle \right) \\ &\leq \max_j \min(\|\Delta_p(\mathcal{X}_j)\|_p, \|\Delta_p(\pi_j \mathcal{G})\|_p) \quad \square \end{aligned}$$

Figure 7 shows that the bound of Proposition 4.1 is tight.

PROPOSITION 4.3.

$$\begin{aligned} &\widehat{\mathcal{X}} \subseteq \widehat{\mathcal{G}} \iff \forall x \in \widehat{\mathcal{X}} : x \in \widehat{\mathcal{G}} \\ &\iff \forall x_1 \in \mathcal{X}_1, \dots, x_\beta \in \mathcal{X}_\beta : \bigwedge_{j=1}^{\beta} x_j \in \mathcal{G}_j \\ &\iff \bigwedge_{j=1}^{\beta} \forall x_j \in \mathcal{X}_j : x_j \in \mathcal{G}_j \iff \bigwedge_{j=1}^{\beta} \mathcal{X}_j \subseteq \mathcal{G}_j \quad \square \end{aligned}$$

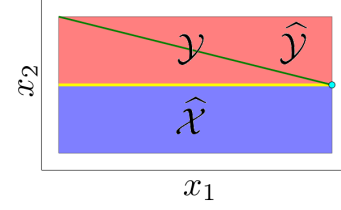


Figure 7. The rectangle $\widehat{\mathcal{X}}$ (blue) and the line segment $\widehat{\mathcal{G}}$ (green) intersect in a single point (cyan). The Cartesian decomposition $\widehat{\mathcal{G}}$ of $\widehat{\mathcal{G}}$ (red) intersects with $\widehat{\mathcal{X}}$ on a whole facet (yellow). Observe that the length of this intersection facet is determined by the width of both $\widehat{\mathcal{X}}$ and $\widehat{\mathcal{G}}$ in dimension x_1 , independent of the height in dimension x_2 .

PROPOSITION 4.4. Let $d \in \mathbb{R}^n$. We show $\rho_{\text{CH}(\widehat{\mathcal{X}} \cup \widehat{\mathcal{G}})}(d) \leq \rho_{\times_j \text{CH}(\mathcal{X}_j \cup \mathcal{G}_j)}(d)$.

$$\begin{aligned} &\rho_{\text{CH}(\widehat{\mathcal{X}} \cup \widehat{\mathcal{G}})}(d) = \max(\rho_{\widehat{\mathcal{X}}}(d), \rho_{\widehat{\mathcal{G}}}(d)) \\ &= \max \left(\sum_j \rho_{\mathcal{X}_j}(d_j), \sum_j \rho_{\mathcal{G}_j}(d_j) \right) \leq \sum_j \max(\rho_{\mathcal{X}_j}(d_j), \rho_{\mathcal{G}_j}(d_j)) \\ &= \sum_j \rho_{\text{CH}(\mathcal{X}_j \cup \mathcal{G}_j)}(d_j) = \rho_{\times_j \text{CH}(\mathcal{X}_j \cup \mathcal{G}_j)}(d) \quad \square \end{aligned}$$

PROPOSITION 4.5. The first bound is due to Proposition 2.1.

$$\begin{aligned} &d_H^p(\text{CH}(\widehat{\mathcal{X}} \cup \widehat{\mathcal{G}}), \times_j \text{CH}(\mathcal{X}_j \cup \mathcal{G}_j)) \\ &= \max_{\|d\|_p \leq 1} \rho_{\times_j \text{CH}(\mathcal{X}_j \cup \mathcal{G}_j)}(d) - \rho_{\text{CH}(\widehat{\mathcal{X}} \cup \widehat{\mathcal{G}})}(d) \\ &= \max_{\|d\|_p \leq 1} \left(\sum_j \rho_{\text{CH}(\mathcal{X}_j \cup \mathcal{G}_j)}(d_j) \right) - \max(\rho_{\widehat{\mathcal{X}}}(d), \rho_{\widehat{\mathcal{G}}}(d)) \\ &= \max_{\|d\|_p \leq 1} \left(\underbrace{\sum_j \max(\rho_{\mathcal{X}_j}(d_j), \rho_{\mathcal{G}_j}(d_j))}_{=: \varphi(d_j)} \right) - \max \left(\sum_j \rho_{\mathcal{X}_j}(d_j), \sum_j \rho_{\mathcal{G}_j}(d_j) \right) \\ &= \max_{\|d\|_p \leq 1} \min \left(\sum_j \varphi(d_j) - \rho_{\mathcal{X}_j}(d_j), \sum_j \varphi(d_j) - \rho_{\mathcal{G}_j}(d_j) \right) \\ &= \max_{\|d\|_p \leq 1} \min \left(\sum_j \max(0, \rho_{\mathcal{G}_j}(d_j) - \rho_{\mathcal{X}_j}(d_j)), \sum_j \max(0, \rho_{\mathcal{X}_j}(d_j) - \rho_{\mathcal{G}_j}(d_j)) \right) \\ &\leq \max_{\|d\|_p \leq 1} \sum_j |\rho_{\mathcal{X}_j}(d_j) - \rho_{\mathcal{G}_j}(d_j)| \quad \square \end{aligned}$$